# Stability and Rendering Limitations of a Parallel Hybrid Active-Passive Haptic Interface

Patrick Dills, *Student Member, IEEE*, Alexander Dawson-Elli, Kreg Gruben, Peter Adamczyk, *Member, IEEE*, Michael Zinn, *Member, IEEE* 

Abstract— Impedance based kinesthetic haptic devices have been a focus of study for many years. Factors such as delay and the dynamics of the device itself affect the stable rendering range of traditional active kinesthetic devices. A parallel hybrid actuation approach, which combines active energy supplying actuators and passive energy absorbing actuators into a single actuator, has recently been experimentally shown to increase the range of stable virtual stiffness a haptic device can achieve when compared to the active component of the actuator alone. This work presents both a stability and rendering range analysis that aims to identify the mechanisms and limitations by which parallel hybrid actuation increases the stable rendering range of virtual stiffness. Increases in actuator stability are analytically and experimentally shown to be linked to the stiffness of the passive actuator.

#### I. Introduction

Actuation has been a persistent challenge since the inception of kinesthetic haptic devices. Many attempts have been made to improve haptic actuators and understand how to present a convincing rendering to a user.

To overcome limitations of traditional active only actuators, researchers turned to what is known as hybrid actuation, or the combination of active and passive actuators. Perhaps the earliest investigations of this include work using fixed external dampers to expand the range of virtual stiffness and damping [1]. [2] expanded upon this work showing that MR brakes could be used as controllable physical dampers and was able to expand the range of stable impedances without many of the negatives of using a fixed damper. Passivity observers and fast acting eddy current dampers were able to dissipate excess energy in haptic devices and again improve control robustness of haptic While these hybrid approaches have demonstrated improvements in rendering range, they can suffer from force artifacts arising from the nonlinear brake characteristics and brake actuation delay that results in poor perceived rendering accuracy, a phenomenon referred to as the sticky-effect.

Recently, we have introduced a new hybrid actuation approach that employs measurement and feedback of real-time brake torques.

\*Research supported by NSF Grant 1830516.

Patrick Dills, Alexander Dawson-Elli, Peter Adamczyk, and Michael Zinn are with the Department of Mechanical Engineering at the University of Wisconsin Madison, Madison, WI 53706 USA (e-mail: pdills|dawsonelli| peter.adamczyk|mzinn@wisc.edu).

Kreg Gruben, is with the Department of Kinesiology at the University of Wisconsin Madison, Madison, WI 53706 USA (e-mail: kreg.gruben@wisc.edu).

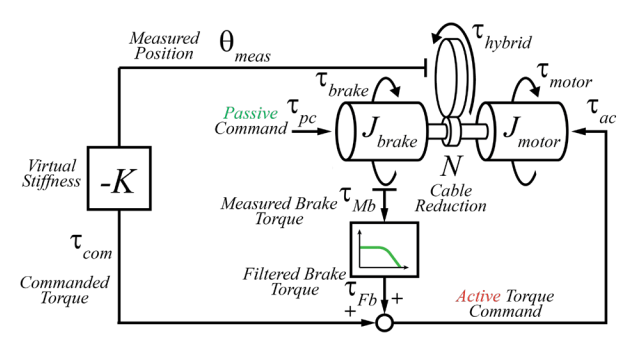


Fig. 1) Schematic representation of the parallel hybrid actuation approach with passive actuator, active actuator, and filtered passive feedback.

Brake torque measurements are used to remove unwanted force artifacts, improving rendering accuracy while maintaining the extended rendering range associated with hybrid devices. Our work in handheld [4] and grounded kinesthetic haptic devices [5] has experimentally shown the range of pure virtual stiffness is increased by combining a particle brake and a DC motor according to the parallel feedback control structure shown in Fig. 1. However, the mechanism by which this arrangement extends the stable rendering range is not well understood. The nonlinear characteristics of passive actuators, in our case a particle brake, are complex, offering various explanations. Some prior work has suggested that a brake's small-deflection stiffness contributes to the extended rendering range [5]. While other hybrid actuation approaches show that dissipation provided by the passive actuator extends a hybrid actuator's rendering range [2], [6]. The work presented here attempts to gain a deeper understanding of the mechanism by which this parallel arrangement of active and passive actuators, shown in Fig. 1, expands the range of stable virtual stiffness. We hope that this ultimately informs and improves the design of future hybrid and parallel actuated systems. Our work is organized as follows:

- Section II: Provides an overview of the assumptions used to model our hybrid actuator, schematically shown in Fig.
   A modified Dahl model and equivalent stiffness and damping analysis form the basis of our modeling assumptions and lends to linear analysis methods.
- Sections III-IV: We analyze the stability of our actuator from the viewpoint of passivity and uncoupled asymptotic stability, starting from the small amplitude model presented in Fig. 2(c). Subsequently, we study the effect of larger perturbations or amplitudes of oscillation on the stability of the system.
- Section V: We present a study of the devices output impedance and factors that affect the output impedance.
- Section VI: We experimentally validate stability results presented in prior sections.

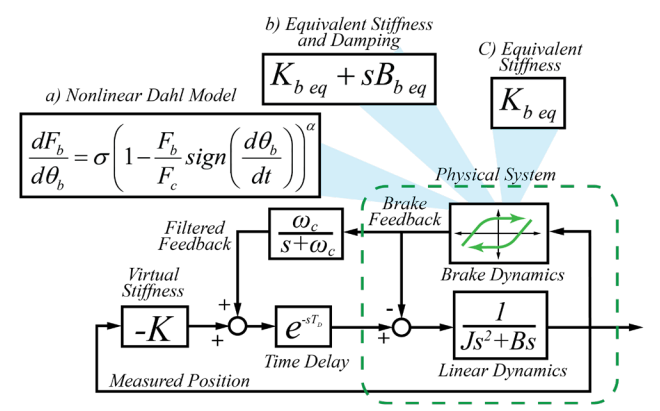


Fig. 2a) Full single degree of freedom Nonlinear model b) Large amplitude linearized model c) Small amplitude linearized model.

#### II. HYBRID ACTUATOR DYNAMICS AND MODELING

Analysis of our hybrid actuator begins with a nonlinear model of a one degree of freedom system which can be seen in Fig. 2. The nonlinear model includes a parallel actuation structure which allows the active actuator to compensate for the passive actuator using measured brake torque. Other model elements, incorporated due to their significant impact on rendering stability, include time delay (to capture sample-and-hold delay and communication delays), a low pass filter in the passive actuator feedback signal (required for noise attenuation), linear inertia and damping plant dynamics, and a nonlinear Dahl friction model which, as shown in [4], captures the important dynamics of the particle brake. For more information about the full parallel actuation approach see [4] and [5].

In our stability and impedance analysis, we have made several simplifying assumptions. We assume that the virtual stiffness is rendered bilaterally, recognizing that this will likely result in conservative stability estimates. Prior literature [7] has equated the bilateral case to steady state contact interior to a virtual wall. Breaking contact with the wall will reduce control forces to zero and maintains stability as a result. Additionally, we assume that the particle brake's Dahl friction model can be represented by an amplitude dependent equivalent stiffness and damping as shown in appendix A. For very small displacements, the equivalent model reduces to a stiffness alone (see Fig. 2(c)). This assumption is valid because nonlinear friction type models have amplitude dependent damping which decreases to zero at zero amplitude [8]. The equivalent stiffness and damping assumptions allow us to apply linear stability analysis to the system and examine the effect of larger amplitude motions on the stability of the actuator.

# A. Equivalent Stiffness and Damping

Assuming a constant brake activation level (corresponding with the steady state frictional force) we can approximate the brake through an equivalent stiffness and equivalent damper in parallel. Several important brake characteristics emerge upon calculating equivalent stiffness and damping (Appendix A). First, the Dahl model simplifies to a pure stiffness at low amplitudes. This is consistent with prior literature studying the Dahl model [8] and motivates the small amplitude linear model presented in Fig. 2(c). Upon reaching larger amplitudes the equivalent stiffness begins to

decrease and damping increases to a critical amplitude where it peaks and begins to decrease. The increase in damping and corresponding decrease in stiffness is also typical to dissipative friction like nonlinearities. Adding an equivalent damping term to the linear model as in Fig. 2(b) allows us to approximately analyze stability of the system at larger amplitudes without the introducing the complexity of the full nonlinear model.

#### III. HYBRID ACTUATOR STABILITY ANALYSIS

Analyzing the stability of the hybrid actuator will highlight the mechanisms that extend and limit the actuator's rendering performance. In this first section, we will consider the effects of time delay, along with the brakes dynamics but ignore the effect of brake measurement filtering, which will be considered in Section III.D.

# A. Small Amplitude Passivity with Unfiltered Passive Actuator Feedback

Considering the system shown in Fig. 2c, where the brake is approximated by an equivalent stiffness, we can evaluate the stability of the system using passivity. Passivity stems from the study of what are known as dissipative or positive real systems [9]. The formal definition of a passive system is shown in (1).

$$\int_{0}^{t} f(\tau)\dot{x}(\tau)d\tau + E(0) \ge 0 \quad \forall t \ge 0$$
 (1)

Variables f and  $\dot{x}$  are conjugate power variables describing energy flow in the system and E(0) is the energy stored in the system at t = 0 [10]. Applying (1) to a one-port system, a single degree of freedom haptic device, like ours implies that a system will be passive if the integral of power extracted from the system over time does not exceed the initial energy of the system [11]. We show this by first calculating the work dissipated by the damper of the system assuming a sinusoidal position, velocity, and time delayed position (2), (3), (4) respectively.

$$x(t) = A\sin(\omega t) \tag{2}$$

$$\dot{x}(t) = A\omega\cos(\omega t) \tag{3}$$

$$x_D(t) = A\sin(\omega t - \omega T_D) \tag{4}$$

The work dissipated by a damper can be calculated from (5) the integral of power over time.

$$W_b = \iint B\dot{x}dx = \iint (B\dot{x})(\dot{x}dt) \tag{5}$$

Substituting (3) for the velocity terms in (5) and integrating over one period of motion yields a symbolic expression (7) for the total work dissipated by linear damping in the system for each cycle of motion.

$$W_b = \int_0^{\frac{2\pi}{\omega}} \left( BA\omega \cos(\omega t) \right) \left( A\omega \cos(\omega t) \right) dt \tag{6}$$

$$W_b = BA^2 \omega \pi \tag{7}$$

The work due to the actuator force is then calculated by substituting (3) and (4) into (5) and can be seen in (10).

$$W_a = \iint (K - K_b) x_D dx = \iint (K - K_b) x_D (\dot{x} dt)$$
 (8)

$$W_a = \int_0^{\frac{2\pi}{\omega}} F_a \left( A\omega \cos(\omega t) \right) dt \tag{9}$$

$$F_a = (K - K_b) A \sin(\omega t - \omega T_D)$$

$$W_a = -\pi A^2 (K - K_b) \sin(T_d \omega) \tag{10}$$

While the virtual stiffness is greater than the physical stiffness the active actuator is generating energy as we might expect. However, if the virtual stiffness is less than the physical stiffness the active actuator becomes dissipative despite the entire system rendering a net positive stiffness. This is the behavior that allows the system to remain stable and passive independent of delay. To satisfy the passivity integral (1) the sum of the work done must be greater than zero (11).

$$BA^2\omega\pi - \pi A^2 (K - K_b) \sin(T_d\omega) \ge 0 \tag{11}$$

The resulting inequality is most restrictive as the frequency,  $\omega$ , approaches zero. Evaluating the expression at zero frequency results in (12) where  $T_D$  is the delay time, B is the linear damping, and  $K_b$  is the brakes stiffness. Equation (12) bounds the maximum passive virtual stiffness our device can produce. An approximation for the delay due to the zero-order hold ( $T_D = T/2$  sec) yields a passivity relationship in terms of sample time T.

$$K \le \frac{B}{T_D} + K_b \iff K \le \frac{2B}{T} + K_b \tag{12}$$

Several insights into the stability of the system are gained through this simplified analysis and are summarized below:

- 1. **Brake stiffness, K<sub>b</sub>, is an important factor** in determining the range of passive virtual stiffness our hybrid device is capable of rendering, and a higher brake stiffness directly increases the maximum stable virtual stiffness.
- 2. *No physical damping, B, is needed* to passively render virtual stiffness up to the brake's stiffness.
- 3. The range of virtual stiffness reduces to the brake stiffness as time delays increase. The system is *passive independent* of delay for virtual stiffness up to the brake stiffness.

An intuitive explanation for the stability results emerges when considering (12). The parallel actuation topology allows the actuator to *substitute physical stiffness for virtual stiffness*.

B. Asymptotic Stability Independent of Delay

As an alternative approach, we can consider the asymptotic stability of the system shown in Fig. 2c, using pseudo-delay methods [12], [13]. Pseudo-delay methods utilize a mapping based on the bilinear transform to transform the infinite dimensional time delayed system to a finite dimensional system. Stability analysis of the finite dimensional system allows one to draw conclusions about the stability of the original system.

First, we substitute the pseudo-delay (13) for pure delay terms in the systems closed loop transfer function yielding the characteristic quasi-polynomial (14).

$$e^{-sT_D} = \frac{1 - \frac{T}{s}}{1 + \frac{T}{s}} \tag{13}$$

$$JTs^{3} + (J + BT)s^{2} + (B - KT + 2K_{b}T)s + K$$
 (14)

The Routh array, Table 1, can be used to analyze the stability of (14) which now depends on an additional parameter, T, the pseudo-delay. The system will be stable if the first column of the Routh array is positive.

Table 1. Routh array for characteristic quasi-polynomial

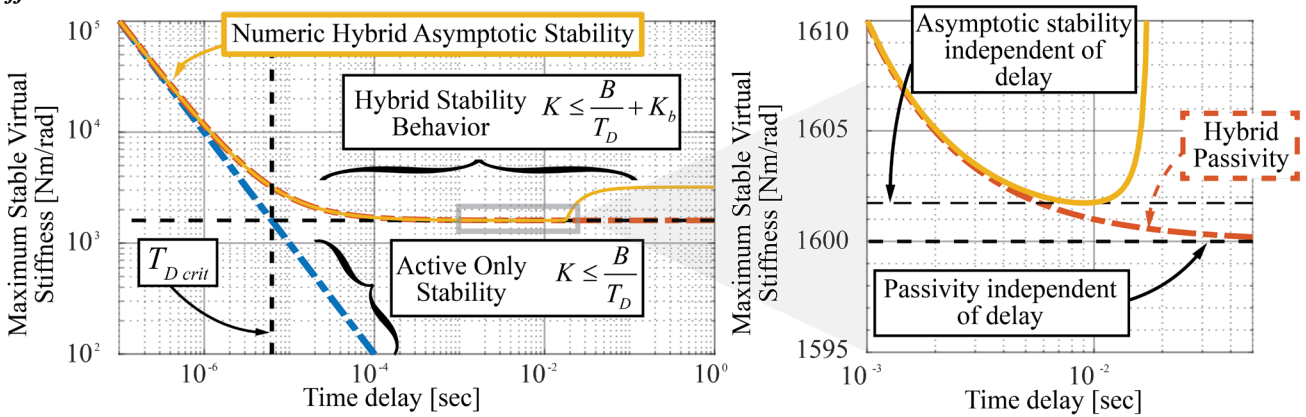
JT	$B-KT+2K_b$
J + BT	K
$\frac{\left(2BK_b - BK\right)T^2 + \left(B^2 - 2JK + 2JK_b\right)T + BJ}{BT + J}$	0
K	0

Considering only positive parameter values leaves (15) as the limiting case. A discriminate analysis allows us to determine the range of values where the system will be stable for all values of the pseudo-delay, *T*.

$$\frac{(2BK_b - BK)T^2 + (B^2 - 2JK + 2JK_b)T + BJ}{BT + J} > 0$$
 (15)

Setting the discriminate equal to zero and solving for the virtual stiffness, K, yields (16), the upper bound for the maximum uncoupled virtual stiffness independent of delay.

$$K \le K_b + \frac{B\sqrt{4JK_b - B^2}}{2J} \tag{16}$$



a) Maximum virtual stiffness of hybrid and active only devices b) Zoomed plot of stability independent of delay Fig. 3a) Plots of maximum stable stiffness vs total time delay. Parameter values used to generate all theoretical curves are found in Table 1 b) Zoomed plot showing a numerical comparison of asymptotic stability to an exact expression obtained via pseudo-delay methods and the passivity expression.

# C. Asymptotic Stability and A Critical Delay

We can compare the stability analyses of the hybrid device to an active only device (where  $K_b = 0$ ) by numerically evaluating the maximum asymptotically stable stiffness using a bisection method, the Nyquist stability criteria, and the systems open loop transfer function (17). Numerical results, excluding filter effects and equivalent damping, shown in Fig. 3, are obtained using the stiff brake parameters from Table 1 in the experimental section VI.

$$OLTF = \frac{e^{-s\left(\frac{T}{2} + T_D\right)}}{Js^2 + Bs + B_b s + K_b - e^{-s\left(\frac{T}{2} + T_D\right)} \left(\frac{\omega_c}{s + \omega_c}\right) \left(B_b s + K_b\right)}$$
(17)

As seen in Fig. 3, the hybrid system outperforms the active system most significantly at lower sample frequencies or large delays. In fact, we can identify a critical delay, from the passivity-based expression (12), in terms of system parameters. For delay larger than the critical delay,  $T_{Dcrit}$ , identified in (18), the hybrid system will outperform the active only system in the sense that the maximum rendered stiffness will be significantly larger.

$$T_{D \ crit} = \frac{B}{K_b} \Leftrightarrow f_{crit} = \frac{K_b}{2B}$$
 (18)

For delay less than  $T_{Dcrit}$ , the hybrid and active only systems have similar performance, although the hybrid device's maximum asymptotically stable virtual stiffness will always achieve a higher stiffness than the active device alone by a quantity of at least the brake stiffness even at very low time delays.

# D. Effects of Filtered Passive Actuator Feedback on Maximum Virtual Stiffness

Prior to this section we have considered a system with ideal passive feedback, where the measured brake force was not filtered. However, an unfiltered passive feedback signal can be difficult to achieve in practice. Filtering may be required due to sensor noise or to prevent aliasing during analogue to digital conversion. The addition of a filter must be done carefully because it has implications on both the stability and output impedance of the actuator.

Evaluating closed form solutions of uncoupled asymptotic stability are not practical for the filtered feedback case with delay, shown in Fig. 2.

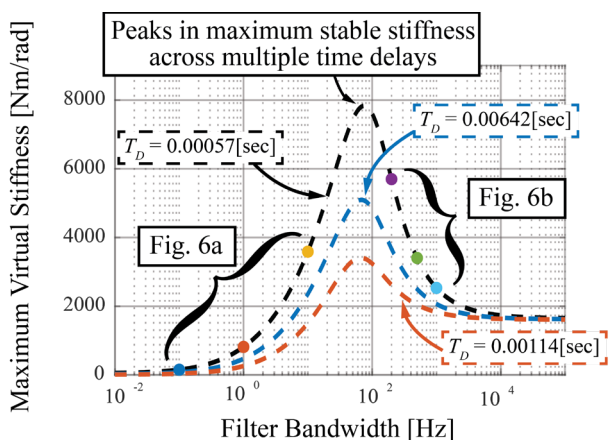


Fig. 4) Numerical maximum stable virtual stiffness while varying the filter cutoff frequency or bandwidth for a range of different time delays.

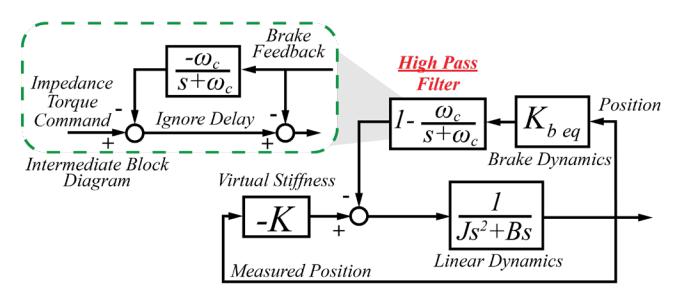


Fig. 5) Reformulated block diagram showing the effect of passive actuator torque and passive actuator feedback resulting in a net high pass filtered position feedback effect on the open loop transfer function.

As such, we numerically evaluate uncoupled asymptotic stability utilizing the open loop transfer function (17) while neglecting equivalent damping, using a bisection method, bode plots, and the Nyquist Stability Criteria (see Fig. 4).

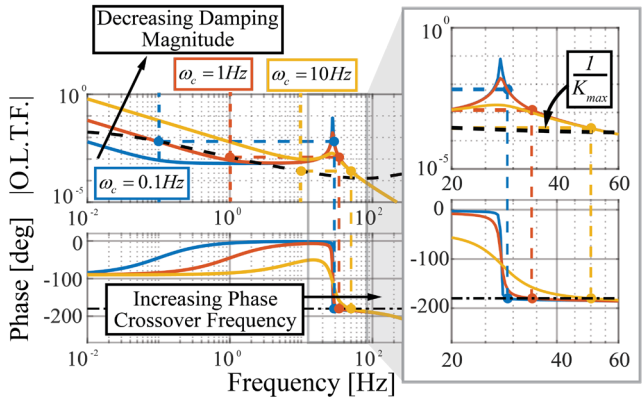
As seen in Fig. 4, the maximum virtual stiffness approaches the active devices stability limit as the filter cutoff frequency approaches zero. Conversely, the maximum virtual stiffness approaches the result obtained for a fixed delay alone (where we assume perfect brake torque measurement) as the cutoff frequency approaches infinity. As seen in Fig. 4, continuously varying the filter cutoff frequency shows a curious peak in the resulting uncoupled stability curve, suggesting that the maximum virtual stiffness can be increased significantly, as compared to the perfect brake measurement case, by selecting a particular brake feedback cutoff frequency.

To gain insight into this phenomenon, it is useful to temporarily ignore delay in the system, which allows us to reorganize our block diagram from Fig. 2 into Fig. 5. As seen in Fig. 5, physical reflected brake torque and the low pass filtered brake feedback signal produced by the active actuator cancel each other at low frequencies. Subtracting a low pass filtered signal from itself results in a high pass filtered signal. High pass filtering a signal in phase with position results in the approximation of a damper below the filter bandwidth.

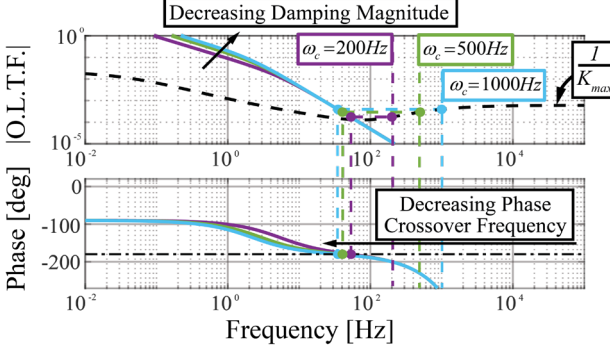
One can use the system's open loop frequency response and the Nyquist stability criteria to better understand why the high pass behavior of the brake and filtered brake feedback allow for increased virtual stiffness. Additionally, we aim to understand why there is an optimal tuning and how one can tune the passive feedback filter to obtain this.

Fig. 6 shows the system's open loop transfer function for a range of filter cutoff frequencies. Fig. 6a shows three frequency responses of the hybrid open loop transfer function corresponding to the portion of Fig. 4, where the maximum virtual stiffness increases as the cutoff frequency increases.

The effect of the combined high pass filter on the maximum stable virtual gain becomes clear with knowledge of the combined high pass hybrid damping effect. As the filter bandwidth increases, damping from the high pass hybrid effect reaches higher frequencies. This helps to both decrease the magnitude of resonance associated with the brake stiffness and smooths the 180-degree phase loss associated with the otherwise lightly damped mode introduced by the brake. These combined effects allow for an increased phase crossover frequency and overall maximum virtual stiffness.



a) Bode plots with increasing maximum virtual stiffness



b) Bode plots with decreasing maximum virtual stiffness Fig. 6a) Bode plots of the open loop transfer function of the system with increasing filter bandwidth while the maximum virtual stiffness is increasing. b) Bode plots of the system with a decreasing maximum virtual stiffness.

Dissipation created by the combined high pass hybrid effect is mostly limited to frequencies below the filters cutoff frequency and decreases in magnitude as the filter bandwidth increases, see Fig. 6b. As the filter cutoff frequency continues to increase, phase loss from external delay in the system begins to dominate added phase from the high pass filter at high frequencies, reducing the phase crossover frequency and the corresponding maximum virtual stiffness. The combined effects of damping, introduced by the filtered brake signal, and a corresponding decrease in damping magnitude, as the cutoff frequency increases, causes the peak in maximum virtual stiffness (see Fig. 4).

The system's internal resonance plays a large role in determining the location (i.e. filter cutoff frequency) of the maximum uncoupled stable virtual stiffness. In fact, we can see that the peak in maximum virtual stiffness and the resonance peak in the open loop transfer function occur at similar frequencies. This is not by chance and moving the physical system's resonance changes both the peak maximum virtual stiffness value and the cutoff frequency needed to achieve the maximum virtual stiffness. In general, shifting the resonance to a lower frequency corresponds to higher peak virtual stiffness. This is because the high pass damping effect is more effective at lower frequencies below its cutoff frequency.

Reducing the resonance frequency, with the intent to increase peak virtual stiffness, can be achieved primarily in two ways. Firstly, brake stiffness could be reduced. However, doing so affects the amount of dissipation achieved through the hybrid high pass filter effect. Device inertia has the most

significant effect on the maximum stiffness in this regard. Increasing inertia shifts the resonance to a lower frequency without reducing energy dissipation in the system, although doing so has negative impacts on device output impedance.

# IV. LARGE AMPLITUDE STABILITY RESULTS

We can analyze the full nonlinear system and investigate its behavior for large amplitude displacements by employing the approximate equivalent stiffness and damping approximation from section IIA.

Expanding our analysis to include equivalent damping as seen in Fig. 2b allows us to analyze the "average" behavior of the hybrid actuator for a given orbit about the equilibrium point. For various amplitudes, we substitute the amplitude dependent stiffness and damping into the full open loop transfer function (17) and solve for the uncoupled asymptotic stability utilizing a combination of the bisection method, bode plots, and the Nyquist Stability. The resulting amplitude dependent stability curve is shown in Fig. 7.

Several important features are evident from Fig. 7, and four distinct regions of stability behavior emerge from this analysis. The system displays unconditional stability across all amplitudes at low stiffness, below the active only asymptotic stability limit. The system is conditionally stable over a range of amplitudes at virtual stiffness below the hybrid small amplitude stability limit. The system has a possibility of limit cycles above the small amplitude stability point for a limited range of amplitudes and virtual stiffness. Finally, at truly large stiffness the device becomes unstable at all amplitudes. The useful rendering range of the hybrid actuator is below the small amplitude asymptotic stability limit, where the system will decay back to an equilibrium point.

It might seem that the conditional stability provided by the hybrid actuator is insufficient, but the interaction forces required to deflect the actuator beyond the maximum amplitude predicted are relatively large and larger brake activation levels can increase the stable range of amplitudes. In practice a modestly sized brake can provide a useful range of conditionally stable amplitudes for the actuator to operate over. For example, the hybrid actuator shown in Fig. 10 can render the stiffness up to 15 Nm of force which corresponds to deflections of approximately 0.3 degrees at its maximum stable stiffness from Fig. 7.

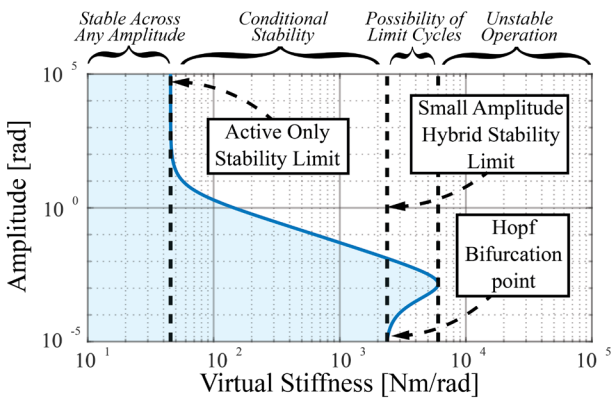


Fig. 7) Amplitude dependent stability curve showing four distinct regions of stability. The curve is generated by substituting equivalent stiffness and damping values into the linear model for a range of position amplitudes.

Some might recognize Fig. 7 to be a form of a bifurcation diagram where the virtual stiffness is the bifurcation parameter. In fact, that is one interpretation of Fig. 7. A Hopf bifurcation can occur at the small amplitude stability limit if filtered feedback is used. While limit cycles are not useful for a haptic device, the behavior can be perplexing for a user or designer of this class of hybrid haptic device. Limit cycles are particularly easy to achieve at low filter bandwidths. Increasing filter bandwidth minimizes the possibility of this behavior as limit cycles are not possible at an infinite filter bandwidth.

# V. LIMITATIONS AND FACTORS ON OUTPUT IMPEDANCE

Typical haptic devices have imperfect renderings due to physical device dynamics including damping, friction, and inertia. These unavoidable features inevitably distort the device's rendering and output impedance. The impedance transfer function for our hybrid device, relative to the device's position, is shown in (19).

$$\frac{\tau_H(s)}{\theta(s)} = Js^2 + Bs + K_b + \left(K - \frac{\omega_c}{s + \omega_c} K_b\right) e^{-sT_d}$$
 (19)

Our hybrid device has physical damping and inertia inherent to the device along with physical stiffness and damping added by the passive actuator. Physical passive actuator dynamics and delay can distort the device's impedance as well. Fig. 8 shows the effect that the feedback filter bandwidth has on device output impedance.

We see, from Fig. 8, that the passive actuator distorts the output impedance when the filter is tuned quite low. Increasing the filter's cutoff frequency effectively reduces distortion below the filter's cutoff frequency. This is only effective at removing distortion due to passive actuator dynamics. Increasing the filter bandwidth has diminishing returns when device dynamics like inertia are primarily responsible for distorting the devices output impedance. Consequently, to present an output impedance equivalent to that of a traditional active only haptic device we must select a filter bandwidth high enough to preserve the devices rendering range.

Fig. 9 shows the effect of delay on the hybrid devices output impedance. At small time delays the output impedance of the device closely matches that of an active device and the desired impedance.

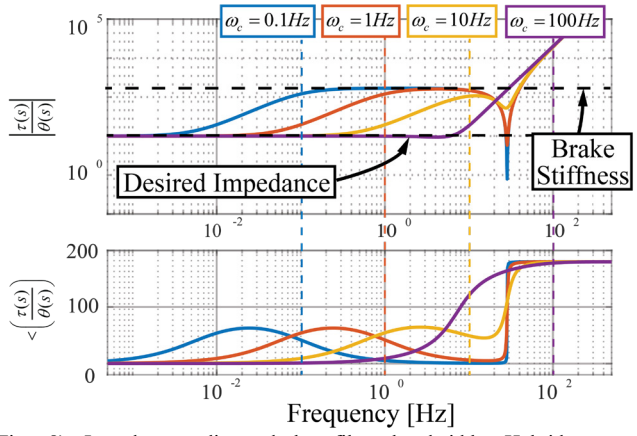


Fig. 8) Impedances distorted by filter bandwidth. Hybrid actuator impedances for a range of filter cutoff frequencies and zero delay.

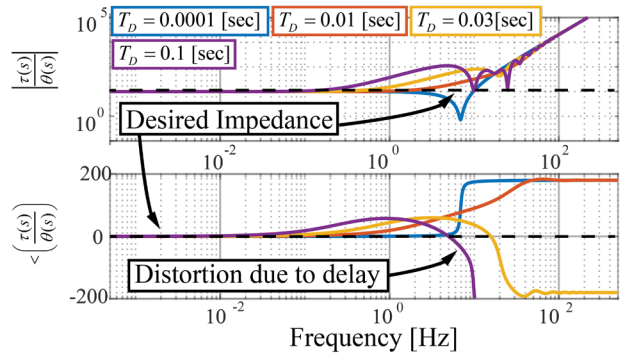


Fig. 9) Impedance frequency response plots distorted by delay. Hybrid actuator impedances for a range of delays and unfiltered passive feedback.

All shown impedances are stable, because the filter bandwidth is infinite for Fig. 9 and the rendered stiffness is less than the brake stiffness. This highlights the fact that it is possible to have significant distortion of a system's impedance due to delay while still maintaining stability. Ultimately, to maintain the desired output impedance, the hybrid actuator needs to have small delays and a sufficient filter bandwidth.

#### VI. EXPERIMENTAL VALIDATION

We validated the stability of the hybrid actuation system using two configurations of a custom one degree of freedom hybrid actuator, shown in Fig. 10.

Our hybrid actuator, shown in Fig. 10a, consists of a Maxon RE90 DC motor, used for the active actuator, and a Placid Industries B6 particle brake as the passive actuator. The actuators are rigidly connected via a capstan and are connected to the output handle via an 11:1 veteran cable transmission. Passive actuator feedback is measured with an Interface MRT-2NM reaction torque sensor. The handle position is measured with a Renishaw Magnetic Linear Encoder, 450,000 lines per revolution, and is used to render the virtual stiffness. This actuator test configuration represents a high brake stiffness configuration typical of a hybrid haptic device designed to extend the maximum stiffness above an equivalent active only device.

Fig. 10b shows a compliant brake configuration where we use a grounded spring as a stand in for a brake, primarily for the purpose of validating high brake filter cutoff frequency experiments which are not practical with the high stiffness configuration.

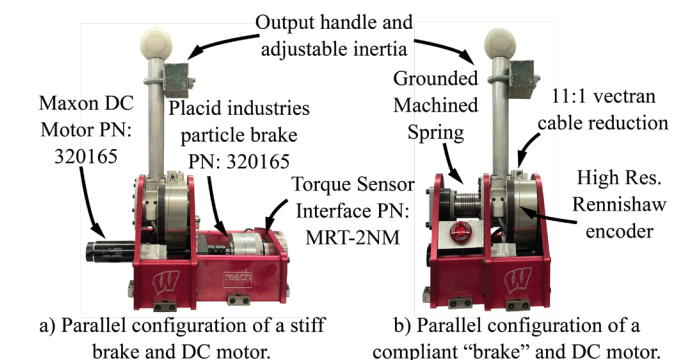


Fig. 10a) The one degree of freedom hybrid actuator used to test the hybrid actuation approach. The device includes a DC Motor and a Particle Brake rigidly connected in parallel. b) A "compliant brake" configuration utilizing a grounded machined spring as a stand in for the particle brake.

Table 2 lists the estimated hybrid device parameters for both compliant and stiff break configurations.

Table 2. Summary of Hybrid Parameters

<u> </u>					
Parameter	Brake Stiffness	Spring Stiffness	Inertia	Damping	
Value	1600	14	0.053	0.013	
Units	[Nm/rad]	[Nm/rad]	[Nm/(rad/sec2)]	[Nm/(rad/sec)]	

# A. Hybrid Stability Validation - Stiff Brake Configuration

We begin our experimental validation by testing the uncoupled stability of a prototype desktop hybrid actuator, using the high brake stiffness configuration, and comparing it to our theoretical results.

During the experiment, we incrementally increased the virtual stiffness of the hybrid actuator. An active disturbance signal was injected onto the motor torque command to perturb the system. The system was also manually perturbed with a dead blow hammer. The tested virtual stiffness is considered to be stable if no vibrations or unstable behavior are detected after four perturbations, spaced two seconds apart. The virtual stiffness is then increased randomly, in a predetermined range. This process is repeated until unstable behavior, vibrations or oscillations, are observed.

We tested five delays while running our system with a 3500 Hz sample frequency. The nominal experimental system delay, including the effects of sampling and processing, was measured at 0.0003 seconds. We added additional delay between 0.01 and 0.0001 seconds. Fig. 11 shows a comparison between the maximum stable stiffness when using the high brake stiffness configuration of the hybrid actuator and the maximum stable stiffness when using the active actuator stiffness configuration. The results from a series of five tests compare well to the theoretical results and are well above the theoretical active only stability curve at the delays used.

Varying the filter bandwidth was also identified as an important factor affecting the maximum stable virtual stiffness. Noise propagation in the high brake stiffness system limits the experimental validation to filter cutoff frequencies less than approximately 30 Hz. Fig. 12 compares the theoretical hybrid curve (for zero added delay) to a range of experimentally obtained maximum stiffness values over a range of filter cutoff frequencies.

Experimental results from both varying time delay and filter bandwidth agree well with the linear analysis and deviations at lower filter cutoff frequencies are likely due to brake energy dissipation at larger amplitudes.

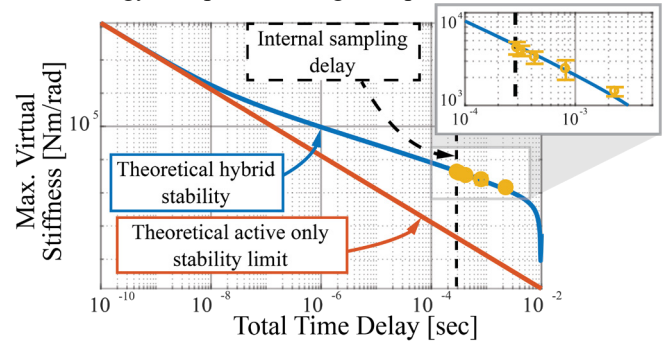


Fig. 11) Experimental stability results for a "stiff" brake (Fig 10a) under varying time delays. Filtered passive actuator feedback of 15 Hz BW is used.

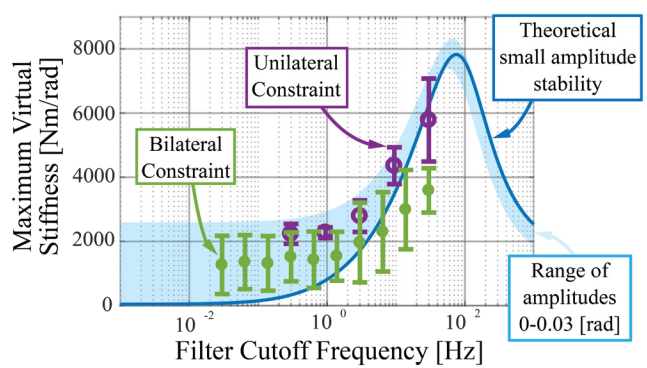


Fig. 12) Theoretical maximum stable virtual stiffness while varying the feedback filter bandwidth. Experimental unilateral and bilateral tests are also plotted over the theoretical curves. Light blue shaded regions are the stable range of amplitudes for a range of oscillation amplitudes (from the large amplitude model).

Additionally, Fig. 12 shows experimental coupled stability results, where the actuator was tested using a unilateral constraint and a human user. Trends predicted in our analysis are reflected in unilateral coupled stability tests as well and we see an increase in the maximum stable virtual stiffness as filter cutoff frequency is increased to 30 Hz.

# B. Hybrid Stability Validation – Compliant Brake Configuration

We present an additional experimental system validation utilizing a compliant brake configuration shown in Fig. 10b. We chose to test a low stiffness brake configuration primarily to allow for validation of the stiffness vs filter bandwidth curve at higher filter bandwidth values. In addition, using a linear spring as a substitute for the small displacement brake stiffness provides the best possible comparison to the presented linear analysis. Finally, measuring spring deflection with a high-resolution encoder eliminates noise issues from torque sensor feedback allowing us to explore a wider range of filter cutoff frequencies.

Fig. 13 shows a comparison between theoretical and experimental results for an unfiltered passive feedback configuration and shows close agreement. The system is stable approximately up to the brake or spring stiffness even under conditions with large time delays.

We see from Fig. 14 that the peak stable stiffness predicted by our analysis, across three sample frequencies or time delays, agrees well both in terms of the predicted filter cutoff frequency and the maximum predicted stable stiffness.

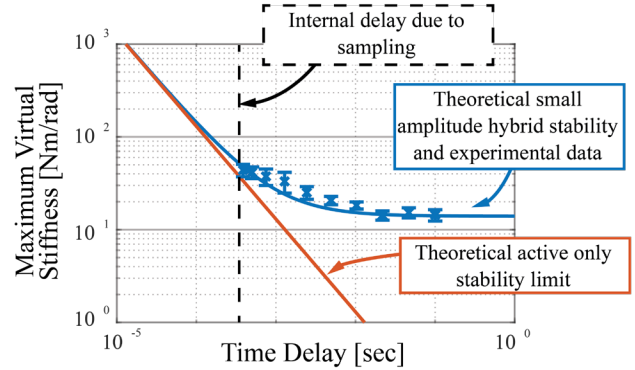


Fig. 13) Experimental stability results under increasing time delays and unfiltered feedback with a compliant brake (Fig 10b).

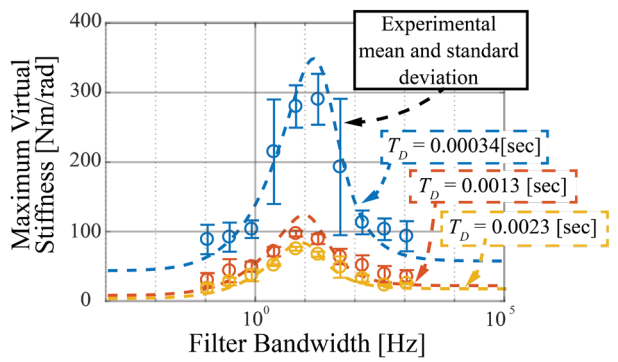


Fig. 14) Maximum stable stiffness for varying filter cutoff frequencies at three different delay values. Experimental results are shown with the mean and standard deviation from six experimental test runs.

Experimental results from the compliant configuration validates the theoretical predictions made in section III and shows that the peak in maximum stable virtual stiffness can be explained through our analysis.

#### VII. CONCLUSION AND FUTURE WORK

Our analysis and experimental validation indicate that the spring-like characteristics of our passive actuator are responsible for the expanded rendering range of the parallel hybrid actuation approach investigated in this work. Carefully tuned filtered passive actuator feedback has been shown to increase the maximum passive and uncoupled virtual stiffness.

This work focused on rendering virtual stiffness. Future work will expand our analysis to a wider set of virtual impedances, including virtual damping, and could yield advancements in hybrid actuator Investigating whether the results translate to a multi-degree of freedom device would also make a meaningful contribution. Overall, we hope that this study of parallel hybrid actuators will inform the design and analysis of future haptic devices and more broadly parallel robotic actuators.

# **APPENDIX**

#### A. Equivalent Stiffness and Damping

Equivalent stiffness and damping can be calculated by first assuming a displacement and resulting velocity (20) and (21) respectively.

$$x = A\cos(\omega t) \tag{20}$$

$$\dot{x} = -\omega A \sin\left(\omega t\right) \tag{21}$$

We can then calculate the time domain waveform of the Dahl model  $F_f(t)$  and find the first two Fourier coefficients (22) and (23).

$$a = \frac{2}{T} \int_{-\frac{T}{2}}^{\frac{T}{2}} F_f(t) \cos(\omega t) dt$$

$$b = \frac{2}{T} \int_{T}^{\frac{T}{2}} F_f(t) \sin(\omega t) dt$$
(22)

$$b = \frac{2}{T} \int_{-T}^{\frac{T}{2}} F_f(t) \sin(\omega t) dt$$
 (23)

Recognizing that equivalent stiffness and damping are forces proportional to displacement and velocity we can equate the Fourier coefficients to our assumed position and velocity waveforms resulting in (24) and (25).

$$a\cos(\omega t) = K_{eq}A\cos(\omega t) \tag{24}$$

$$b\sin(\omega t) = -B_{eq}\omega A\sin(\omega t) \tag{25}$$

Solving (24) and (25) for the equivalent stiffness and damping results in amplitude dependent parameters (26) and (27) respectively.

$$K_{eq} = \frac{a}{A} \tag{26}$$

$$B_{eq} = \frac{-b}{\omega A} \tag{27}$$

#### ACKNOWLEDGMENT

This work was supported by the National Science Foundation under Grant NSF 1830516.

#### REFERENCES

- [1] J. E. Colgate and J. M. Brown, "Factors affecting the Z-Width of a haptic display," in Proceedings of the 1994 IEEE International Conference on Robotics and Automation, San Diego, CA, USA, 1994, pp. 3205-3210. doi: 10.1109/ROBOT.1994.351077.
- J. An and D.-S. Kwon, "Stability and Performance of Haptic Interfaces with Active/Passive Actuators—Theory and Experiments," Int. J. Robot. Res., vol. 25, no. 11, pp. 1121-1136, Nov. 2006, doi: 10.1177/0278364906071034.
- A. H. C. Gosline and V. Hayward, "Time-Domain Passivity Control of Haptic Interfaces with Tunable Damping Hardware," in Second Joint EuroHaptics Conference and Symposium on Haptic Interfaces for Virtual Environment and Teleoperator Systems (WHC'07), Tsukuba, Japan, Mar. 2007, pp. 164-179. doi: 10.1109/WHC.2007.116.
- P. Dills, N. Colonnese, P. Agarwal, and M. Zinn, "A Hybrid Active-[4] Passive Actuation and Control Approach for Kinesthetic Handheld Haptics," in 2020 IEEE Haptics Symposium (HAPTICS), Crystal City, VA, USA, Mar. 2020, pp. 690-697. doi: 10.1109/HAPTICS45997.2020.ras.HAP20.12.af578b0a.
- C. Parthiban, P. Dills, I. Fufuengsin, N. Colonnese, P. Agarwal, and M. Zinn, "A Balanced Hybrid Active-Passive Actuation Approach for High-Performance Haptics," in 2019 IEEE World Haptics Conference (WHC), Tokyo, Japan, Jul. 2019, pp. 283-288. doi: 10.1109/WHC.2019.8816146.
- M. Antolini, O. Kose, and H. Gurocak, "A first order transfer function to balance the workload in brake-motor hybrid actuators," in 2014 IEEE Haptics Symposium (HAPTICS), Houston, TX, USA, Feb. 2014, pp. 509-514. doi: 10.1109/HAPTICS.2014.6775508.
- N. Diolaiti, G. Niemeyer, F. Barbagli, and J. K. Salisbury, "Stability of Haptic Rendering: Discretization, Quantization, Time Delay, and Coulomb Effects," IEEE Trans. Robot., vol. 22, no. 2, pp. 256-268, Apr. 2006, doi: 10.1109/TRO.2005.862487.
- P. R. Dahl, "Solid Friction Damping of Mechanical Vibrations," AIAA J., vol. 14, no. 12, pp. 1675–1682, Dec. 1976, doi: 10.2514/3.61511.
- J.-J. E. Slotine and W. Li, Applied nonlinear control. Englewood Cliffs, N.J: Prentice Hall, 1991.
- [10] J. J. Abbott and A. M. Okamura, "Effects of position quantization and sampling rate on virtual-wall passivity," IEEE Trans. Robot., vol. 21, no. 5, pp. 952-964, Oct. 2005, doi: 10.1109/TRO.2005.851377.
- [11] D. Weir and J. Colgate, "Stability of Haptic Displays," in Haptic Rendering, M. Otaduy, Ed. A K Peters/CRC Press, 2008, pp. 123-156. doi: 10.1201/b10636-9.
- K. Walton and J. E. Marshall, "Direct method for TDS stability analysis," IEE Proc. Control Theory Appl., vol. 134, no. 2, p. 101, 1987, doi: 10.1049/ip-d.1987.0018.
- K. Gu, V. L. Kharitonov, and J. Chen, "Stability of Time-Delay Systems,"